Frontiers in Heat and Mass Transfer (FHMT), 18, 1 (2022)
DOI: 10.5098/hmt.18.1

Global Digital Central
ISSN: 2151-8629

Frontiers in Heat and Mass Transfer

Available at www.ThermalFluidsCentral.org

THE EFFECTS OF WINGLET VORTEX GENERATOR POSITION IN RECTANGULAR-DUCT-TYPE SOLAR AIR HEATERS

Boonchai Lertnuwat

Advanced Computational Fluid Dynamics Research Unit, Department of Mechanical Engineering, Faculty of Engineering, Chulalongkorn University, Bangkok, 10330 THAILAND

ABSTRACT

The aim of this work is to numerically investigate the effect of mounting winglet vortex generators on different positions in rectangular-duct-type air heaters. The two investigated positions were the absorber plate and the insulation plate, opposite to the absorber plate. Four shapes of winglet vortex generator, i.e. perforated rectangular winglet vortex generators (P-RWVG), rectangular winglet vortex generators (RWVG), perforated trapezoidal winglet vortex generators (P-TWVG) and trapezoidal winglet vortex generators (TWVG), were used. Results showed that heat-transfer capability would be better if the winglet vortex generators were mounted on the opposite insulation plate in the cases of P-RWVG, RWVG and P-TWVG.

Keywords: *Solar air heater, Vortex generators, Vortex generator positions, Absorber plate, Nusselt number*

1. INTRODUCTION

Unlike fossil fuels, renewable energy is unlimited and clean .The sources of renewable energy, namely geothermal, hydro energy, wind power, biomass, and solar energy, have long been a major global issue for decades .Their sustainability and non-toxic emissions are great advantages, making them relatively cost-efficient and environmentally friendly. Governments around the world have consequently promoted the usage of renewable energy sources instead of limited and toxic fossil fuels .Solar energy, which is an energy source of renewable energy, has long been harnessed .Since the sun releases both light and heat, there are many methods to make use of its energy; for example, solar electricity, solar ventilation, solar thermal energy for refrigeration or air conditioning and solar heating .

Heating with solar energy needs solar collectors to absorb solar energy and convert it to heat .Then the heat is used to heat either water or air, which are working fluids. The working fluids are finally utilized for specific objectives .For solar air heating, solar collectors are roughly categorized into two groups, i.e. photovoltaic (PV) and solar air heater (SAH). A typical SAH is principally composed of a heat exchanger, a blower and connecting pipes as shown in Fig. 1(a). The heat-exchanging parts of SAHs can be constructed with pipes or tubes (Afshari *et al.*, 2020) but rectangular ducts or channels, as shown in Fig. 1(b), have often been used in solar-energy harvesting systems owing to the larger areas of their solar-energy absorbers (Dezan *et al*., 2020; Ghritlahre *et al*., 2020; Thianpong *et al*., 2009; Xiao *et al*., 2020). A conventional rectangular-duct-type heat exchanger generally consists of four walls .One of them is the solar-energy absorber, so-called absorber plate, as illustrated in Fig.1. The absorber plate could be positioned as either the upper or lower wall. For instance, absorber plates were assigned as upper walls in the work of Ghritlahre *et al.* (2020), Leander Antony *et al.* (2020) and Skullong *et al.* (2018), but were assigned as lower walls in the work of Abdullah *et al.* (2020), Alam *et al.* (2014), Boulemtafes-Boukadoum *et al.* (2019), Gopi *et al.* (2021) and Korpale *et al.* (2020). While the other walls are customarily insulation walls .

Although heat exchange ducts, composed of four smooth-flat plates, have long been developed for several years (Madhwesh *et al.*, 2019), many surface roughness variants have been proposed for mounting on the walls of the heat exchange ducts of high-performance SAHs in order to produce strong longitudinal vortex flows inside the heat exchangers, resulting in faster rates of heat transfer. Grooves and dimples are surface variations which do not intrude the flow fields inside heat exchangers, and have been selected for use in some work (Eiamsa-ard *et al.*, 2008; Liu *et al*., 2015). Some kinds of surface roughness intrude the flow fields inside the heat exchangers to increase heat transfer rates; for example, ribs, fins and winglets. Ribs have been utilized in many projects (Aharwal *et al.*,2008; Bansal *et al.*, 2020; Barik *et al.*, 2021; Patel *et al.*, 2020; Komolafe *et al.*, 2019; Kumar and Layek, 2019a; Kumar *et al.*, 2019; Mahanand and Senapati, 2020; Wang *et al.*, 2020). But some researchers have exploited fins (Hassan *et al.*, 2021; Hosseini *et al.*, 2019; Murali *et al.*, 2020; Singh and Negi, 2020), whereas winglets were used in the work of Dezan *et al.* (2020), Kumar and Layek (2020a) and Kumar and Layek (2020b). Although baffles have regularly been employed to control the flow direction in heat exchangers, they can also induce the vortex flows, thereby increasing heat transfer rates in the heat exchangers (Luan and Phu, 2020; Tamna *et al.*, 2014). Additionally, some of these roughness geometries could be combined and applied for better heat transfer rates (Saravanakumar *et al*.., 2020).

In rectangular-duct-type SAHs, the above-mentioned roughness geometries were usually only mounted on the absorber plate, which is

*Corresponding author Email: Boonchai.L@Chula.ac.th

Global Digital Central
ISSN: 2151-8629

the solar-energy collecting part of the heater (Abdullah *et al.*., 2020; Alam *et al.*, 2014; Boulemtafes-Boukadoum *et al.*, 2019; Ghritlahre *et al.*, 2020; Gopi *et al.*, 2021; Korpale *et al.*, 2020; Leander Antony *et al.*, 2020; Pandey *et al.*, 2016), although some researchers studied the effects of applying roughness geometries on multiple surfaces (Promvonge *et al.*, 2009; Skullong *et al.*, 2015). However, the literature cited above shows that there has not yet been any research into the consequences of repositioning roughness geometries to the insulation wall, opposite to the absorber plate, as illustrated in Fig. 1(b).

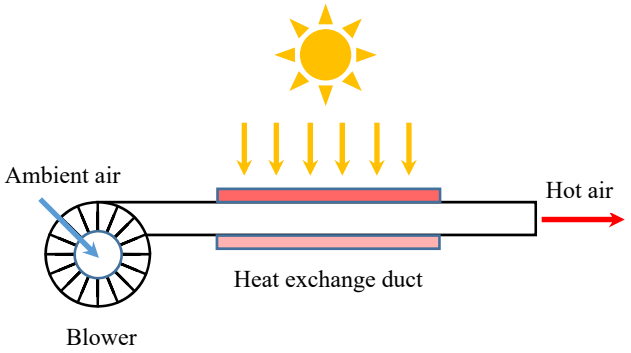

(a) Conventional solar air heater

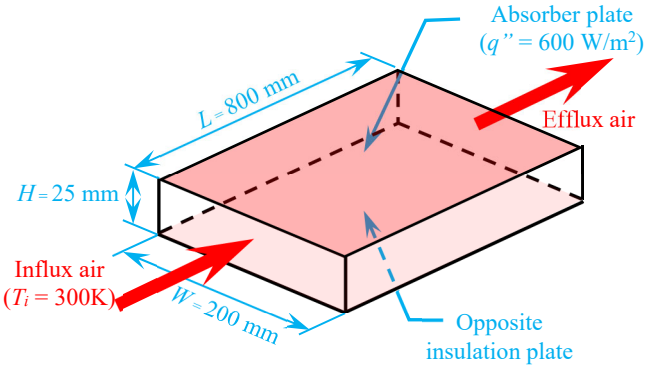

(b) The heat exchange duct of the solar air heater

Fig. 1 Conventional solar air heater and the detail of a heat exchanger duct.

The objective of this work is, thus, to numerically investigate the effects of the positions of winglet vortex generators (WVGs) in rectangular-duct-type SAHs on the capacity of heat transfer, as indicated by the Nusselt number.

2. EXPERIMENTAL SETUP

The solar air heater, proposed in Skullong *et al.* (2018), was employed for this investigation. There were four types of winglet vortex generators, categorized by the shapes of their winglets as shown with their dimensions in Fig. 2: the perforated rectangular winglet vortex generator (P-RWVG), the rectangular winglet vortex generator (RWVG), the perforated trapezoidal winglet vortex generator (P-TWVG) and the trapezoidal winglet vortex generator (TWVG). All winglet vortex generators had the same height (e = 12 mm) and the same length of longer base edges (c = 25 mm). Both the P-TWVG and the TWVG were right trapezoids, whose longer base edges (c) were 12 millimeters longer than their shorter base edges (c_s = 13 mm).

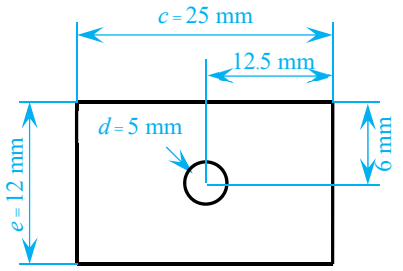

(a) Perforated rectangular winglet vortex generator (P-RWVG)

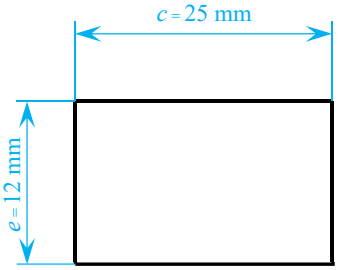

(b) Rectangular winglet vortex generator (RWVG)

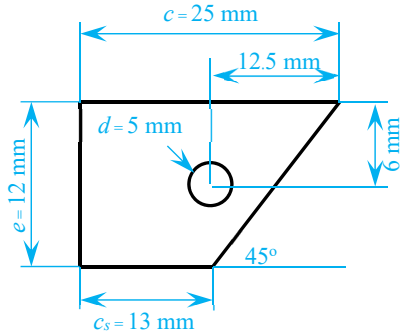

(c) Perforated Trapezoidal winglet vortex generator (P-TWVG)

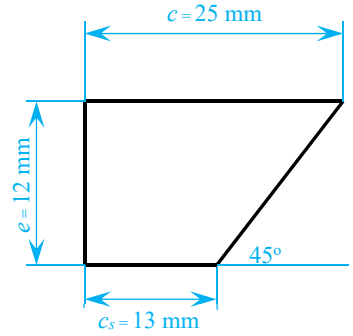

(d) Trapezoidal winglet vortex generator (TWVG)

Fig. 2 The four designs of winglet vortex generators and their dimensions.

As a result of these design variations, the blockage areas of all the vortex generators were different .The punched holes on the perforated

Global Digital Central
ISSN: 2151-8629

winglet vortex generators were circular, with five millimeter diameter (d = 5 mm). The vertical locations of the punched holes were at the middle of the height of both P-RWVG and P-TWVG .The horizontal locations of the punched holes were exactly at the middle of the longer base edges. This means that the punched holes were eccentric to the inclined lateral side in the P-TWVG case.

The setup of the heat exchanging part of the SAH is presented in Fig. 1(b), showing the dimensions of the rectangular heat-exchange duct, the directions of the airflows, the positions of the absorber plate and opposite insulation plate. The dimensions of the heat exchanger are length (L = 800mm), width (W = 200mm) and height (H = 25 mm). Figure 3 shows the 30-degree zigzag arrangement of the winglet vortex generators inside the heat exchange duct .The length of longitudinal pitch (P_l) and the length of transverse pitch (P_t) were 37.5 and 25 mm respectively .These winglet vortex generators could be mounted either on the absorber plate or the opposite insulation plate, depending on the condition of the investigation .

Since the zigzag arrangement creates a periodical flow pattern around the winglet vortex generators, the computational domains in this work were defined to include only the space around a winglet vortex generator, as shown by the green dashed lines in Fig. 3. Three-dimensional computational domains in case of the P-TWVG condition are presented in Fig. 4 as an example of the rest .The winglet vortex generators were approximately mounted with their longer bases at the middle of the longitudinal pitch spacing (P_l). The fixed dimensional parameters of each computational domain were longitudinal pitch spacing (P_l = 37.5 mm), transverse pitch spacing (P_t = 25 mm), duct height (H = 25 mm), winglet height (e = 12 mm), winglet thickness (0.3 mm), attack angle between airflow direction and winglet vortex generator (30°) and, (for perforated winglet vortex generators) punched hole diameter (d = 5 mm). The only difference between Fig. 4(a) and 4(b) is the position of the winglet vortex generator, i.e. the winglet vortex generator is mounted on the absorber plate in Fig. 4(a) whereas it is mounted on the opposite insulation plate in Fig. 4(b) in order to investigate the effect of its position. The present work employed the 3D Cartesian coordinate system, in which the elevation (z = 0) was the position of the opposite insulation plate.

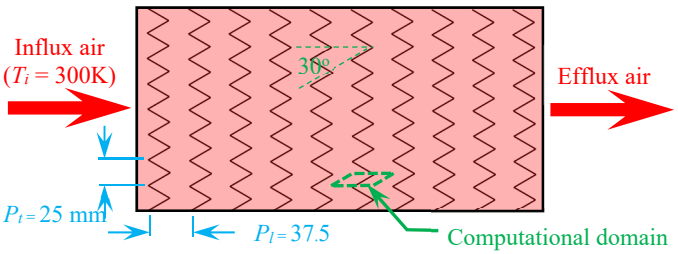

Fig. 3 The zigzag arrangement of the winglet vortex generators, inside the heat exchange duct.

For each computational domain, the absorber plate was posted with the boundary condition of a no-slip wall, releasing constant heat flux (q'') of 600 W/m^2, whereas the opposite plate was a no-slip insulation wall .The left and right boundaries were symmetrical planes. The front and back boundaries were periodical inlets and outlets where constant mass flow rates were maintained in order to achieve six conditions of Reynolds number (Re = 3000, 5000, 7000, 10000, 15000 and 20000), namely

$$\dot{m}_e = \dot{m}_i = \rho \bar{u}_i P_t H / 2 \tag{1}$$

in which the area-averaged velocity of the influx air

$$\bar{u}_i = (\mu Re)/(\rho D) \tag{2}$$

and the hydraulic diameter

$$D = 2(W \times H)/(W + H). \tag{3}$$

At the inlet, the temperature of the air (T_i) was maintained at 300 K.

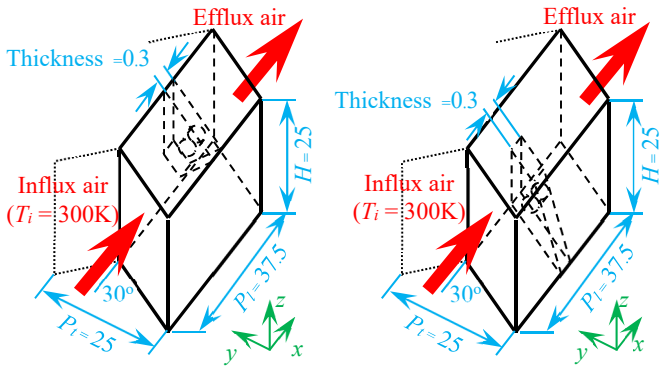

(a) Winglet vortex generator, installed on the absorber plate

(b) Winglet vortex generator, installed on the opposite plate

Fig. 4 The computational domains for flows around perforated trapezoidal vortex generators.

Although most of the winglet vortex generators in the cited literature could conduct heat, the winglet vortex generators in Skullong *et al.* (2018) were treated as insulation plates because they were mounted on the absorber plates with superglue, which is a heat insulator .In addition to the work of Skullong *et al.* (2018), there was also some other research, utilizing insulation winglet vortex generators (Tamna *et al.*, 2014; Tanda, G., 2004). Moreover, Luan, and Phu (2020) found that vortex generators only disturbed the air near the absorber plates where they were mounted, but did not conduct heat to air far away from the absorber plates. Hence, all winglet vortex generator surfaces were assumed to be no-slip heat-insulation walls in the present work .This boundary condition neutralized any effects of heat transfer, resulted from the extended surfaces.

The realizable k-epsilon model, supplemented with a wall function, was selected in this work, as it was suggested in the work of Skullong *et al.* (2018). The assumptions used in the simulations were; (1) thermal radiation was neglected, (2) flows were steady fully developed periodic flows, (3) flows were turbulent and incompressible, (4) body forces were neglected and (5) air was a Newtonian fluid whose properties were density (ρ) = 1.177 kg/m^3, dynamic viscosity (μ) = 1.846 × 10^{-5} kg/m-s, specific heat capacity (C_P) = 1004.9 j/kg-K and thermal conductivity (K) = 0.02624 W/m-K.

3. VERIFICATION OF SIMULATION MODEL

3.1 Parameters of Interest

The two parameters of interest, i.e. the Nusselt number (Nu) and friction factor (f), have often been used to evince the performance of SAHs (Agrawal and Bhagoria, 2021; Kumar and Layek, 2019b; Momin

et al., 2002; Singh *et al*.,2014). Therefore, they were exploited in this work. The Nusselt number is computed from

$$Nu = \bar{h}D/K \ . \tag{4}$$

Herein, $\bar{h}$ stands for the area-averaged convection heat transfer coefficient and is defined as

$$\bar{h} = q''/\left(\bar{T}_{sur} - \bar{T}_{air}\right), \tag{5}$$

where q'' is the constant heat flux of 600 W/m^2 from an absorber plate, $\bar{T}_{sur}$ is the area-averaged temperature of the absorber plate and $\bar{T}_{air}$ is the mass-average temperature of the air in the domain .The friction factor is computed from

$$f = \left[\left(\Delta p/L_P\right)D\right]/\left(\tfrac{1}{2}\rho\bar{u}_i^2\right) \tag{6}$$

where $\bar{u}_i$ is the area-averaged velocity of the influx air andis $\left(\Delta p/L_P\right)$ the area-averaged pressure gradient across the length of the periodic boundaries, which is longitudinal pitch spacing (P_l).

3.2 Criteria of Solution Convergence and Grid Independence

Simulation solutions were accepted when the residual values of all governing equations were less than 10^{-5}. There were two meshes that were exploited to ensure the independence of the grid resolution for each case of the investigation .Coarser and finer meshes respectively consisted of approximately 16000 and 32000 elements .For all cases, the average differences of Nu and f between the coarser and finer meshes were 2.57% and 5.73%, respectively.

3.3 Verification of Simulation Model

The reliability of the simulation model was confirmed by comparing the two parameters of interest (Nu and f), obtained from the simulations, to values, obtained from empirical correlations as follows:

For P-RWVG:

$$Nu = 0.194Re^{0.742}Pr^{0.4}\left(A_h/A_w\right)^{-0.0625} \quad \text{(4.7\% error)}, \tag{7}$$

$$f = 1.814Re^{-0.056}\left(A_h/A_w\right)^{-0.1634} \quad \text{(5.4\% error)}, \tag{8}$$

For RWVG:

$$Nu = 0.347Re^{0.729}Pr^{0.4}\left(B_R\right)^{0.215}\left(P_R\right)^{-0.203} \quad \text{(6.7\% error)}, \tag{9}$$

$$f = 8.334Re^{-0.056}\left(B_R\right)^{0.682}\left(P_R\right)^{-0.525} \quad \text{(7.2\% error)}, \tag{10}$$

For P-TWVG:

$$Nu = 0.191Re^{0.736}Pr^{0.4}\left(A_h/A_w\right)^{-0.0703} \quad \text{(4.9\% error)}, \tag{11}$$

$$f = 1.169Re^{-0.062}\left(A_h/A_w\right)^{-0.1957} \quad \text{(6.2\% error)}, \tag{12}$$

For TWVG:

$$Nu = 0.297Re^{0.736}Pr^{0.4}\left(B_R\right)^{0.13}\left(P_R\right)^{-0.104} \quad \text{(6.9\% error)}, \tag{13}$$

$$f = 5.102Re^{-0.062}\left(B_R\right)^{0.471}\left(P_R\right)^{-0.247} \quad \text{(7.4\% error)}. \tag{14}$$

These empirical correlations were proposed in Skullong *et al.* (2018). The % errors, indicated in each correlation, were the deviations of the predicted data from the empirical equations and the measured data from their experiment. The Prandtl number (Pr) was a constant, equal to 0.7070, and the relevant dimensional parameters are defined as follows:

The area of a punched hole on a perforated winglet vortex generator is

$$A_h = \pi D^2/4 \ . \tag{15}$$

The area of a winglet vortex generator)one side only(is

$$A_w = c \times e \quad \text{for rectangular winglets or}$$
$$A_w = 0.5\left(c + c_s\right) \times e \quad \text{for trapezoidal winglets.} \tag{16}$$

The winglet blockage ratio is

$$B_R = e/H \ . \tag{17}$$

The longitudinal pitch length ratio is

$$P_R = P_l/H \ . \tag{18}$$

Comparisons between simulated results and empirical results, calculated using empirical correlations, are depicted in Fig. 5(a) - (d) as functions of the Reynolds number .The abscissas of the simulation results were the six chosen Reynolds numbers (Re = 3000, 5000, 7000, 10000, 15000 and 20000). The Nusselt numbers, from most of the simulations, were a little less than those of the empirical correlations when the Reynolds number was below 15000, but were a bit greater when the Reynolds number increased beyond this .The exception to this was the case of TWVG because the Nusselt numbers, from the simulations, were almost coincident on the empirical curve .Friction factors, obtained from the simulations, were slightly less than those of the empirical correlations, except the leftmost point in the case of RWVG .These figures show that simulation results were very similar to those of the empirical correlations, and therefore acceptable.

4. RESULTS AND DISCUSSION

4.1 The Effects of Winglet Vortex Generator Position

The percentage of difference between Nusselt numbers, obtained from cases in which the winglet vortex generator is mounted on the absorber plate and in which it is mounted on the opposite insulation plate,

$$\%diff_{Nu} = 100\% \times \left(Nu_{opposite} - Nu_{absorber}\right)/Nu_{absorber} \ , \tag{19}$$

was an indicator of the change in heat-transfer capability when the winglet vortex generators were repositioned .The four curves of $\%diff_{Nu}$ are presented in Fig .6 as functions of Reynolds number .These four curves are categorized by shape of winglet vortex generator .This figure reveals that the positions of the winglet vortex generators significantly affected the capability of heat transfer between absorber plates and airflows in the heat exchange duct .In cases of P-TWVG, P-RWVG and RWVG, $\%diff_{Nu}$ increased when the Reynolds number rose from 3000 to 10000, after which it tended to level off .This implied that $\%diff_{Nu}$ did not depend on Reynolds number when Reynolds number was greater than 10000, for these winglet vortex generators .Because maximum magnitudes of $\%diff_{Nu}$ were much greater than the magnitudes of the % errors that were indicated in empirical correlations, i.e. Eq. (7), Eq. (9) and Eq. (11), it could be inferred that the positions of these winglet vortex generators significantly influence heat transfer capacity in SAHs.

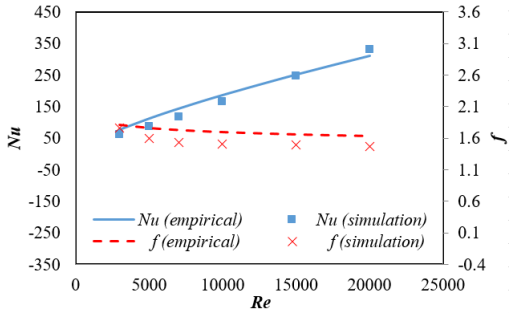

(a) P-RWVG

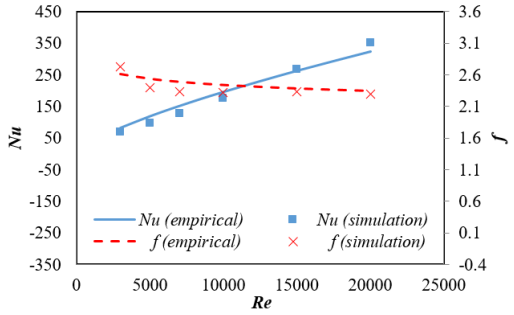

(b) RWVG

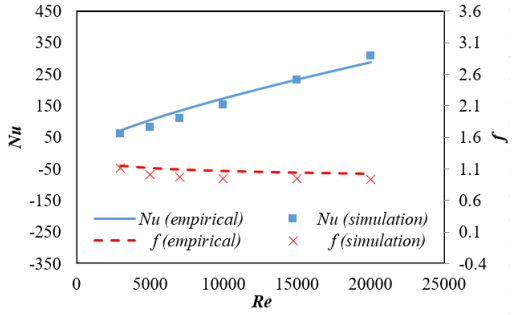

(c) P-TWVG

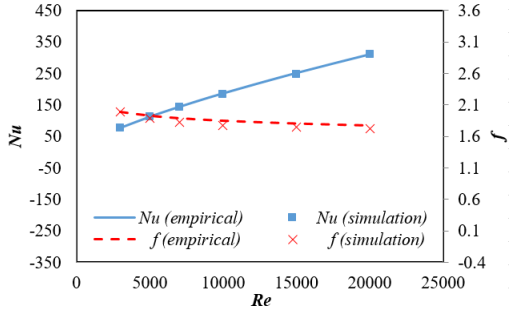

(d) TWVG

Fig. 5 Comparisons between Nusselt numbers (Nu) and friction coefficients (f), obtained from empirical correlations and simulations, as functions of Reynolds number.

The curve of TWVG was different from the others since the value of the $\%diff_{Nu}$ declined from the positive to the negative zone as the Reynolds number increased .The change of the sign) positive and negative(of the $\%diff_{Nu}$ values took place within the region of $5000 < Re < 7000$ .This meant that mounting winglet vortex generators on the opposite insulation plate gave worse heat transfer capabilities when the Reynolds number was higher .Although the magnitudes of the $\%diff_{Nu}$ were not much greater than the magnitude of the% error in the empirical correlation, Eq. (13), the curve of $\%diff_{Nu}$ still decreased as Reynolds number increased .It is, thus, expected that the magnitude of the $\%diff_{Nu}$ would be more significant if the Reynolds number was higher.

In the same way, the percentage of difference between friction factors, obtained with different positions of winglet vortex generator is defined as

$$\%diff_f = 100\% \times \left(f_{opposite} - f_{absorber} \right) \Big/ f_{absorber} \,. \tag{20}$$

Since the simulated airflows were assumed to be incompressible and body forces were neglected, the simulated flow fields were almost independent of winglet vortex generator position for each Reynolds number and winglet vortex generator shape .The only difference between any two simulated flow fields, obtained from the two different positions of winglet vortex generators under the same Reynolds number, was that they were mirror images of each other . Consequently, $\%diff_f$ in all cases was approximately zero. This means that repositioning the winglet vortex generators only affected the heat-transfer capability of SAHs but did not affect friction loss inside the heat exchange duct.

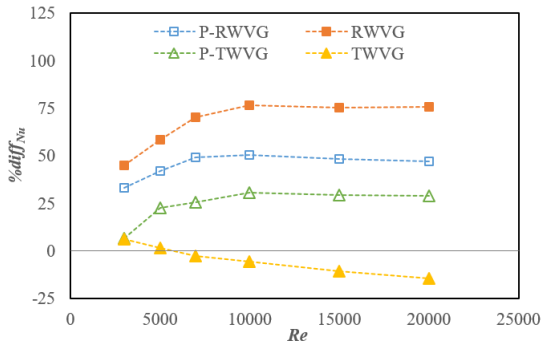

Fig. 6 Percentage differences between Nusselt numbers (from cases in which winglet vortex generators were mounted on absorber plates and in which they were mounted on the opposite insulation plates) for the four different shapes of winglet vortex generator.

4.2 Discussion

The distributions shown in Fig. 7 are the relationships between Reynolds number and turbulent kinetic energy (k), averaged over all computational domains .It was found that domain-averaged k , in cases that P-RWVG, RWVG and P-TWVG were mounted on absorber plates, was much greater than domain-averaged k of TWVG. Domain-averaged , k in cases of winglet vortex generators mounted on opposite insulation plates, were identical to Fig .7; hence they are not depicted here .For the same Reynolds number, the highest domain-averaged k belonged to RWVG, followed by P-RWVG and R-TWVG, whereas the lowest domain-averaged k belonged to TWVG .This order was the same for $\%diff_{Nu}$. However, there is no limiting asymptote for the domain-averaged k curves in Fig. 7, which is different from the $\%diff_{Nu}$ curves for RWVG, P-RWVG and P-TWVG in Fig. 6. The similarities between domain-averaged k and $\%diff_{Nu}$ implied that turbulent kinetic energy played an important role in $\%diff_{Nu}$.

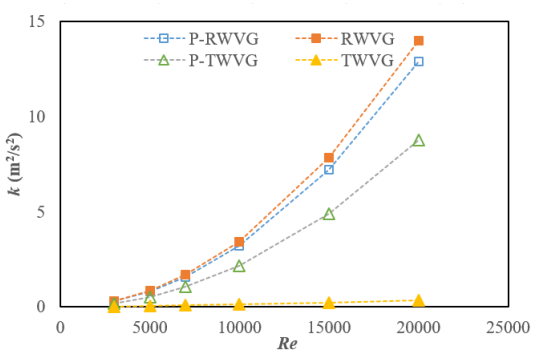

Fig. 7 Relations between Reynolds number and domain-averaged turbulent kinetic energy (k), obtained from cases in which winglet vortex generators were mounted on absorber plates.

In order to evince the important role of turbulent kinetic energy in $\%diff_{Nu}$, the distributions of area-averaged k, plotted against z-axis position, are shown in Figs. 8 - 11. The elevation where $z = 0$ is the position of the opposite insulation plate as shown in Fig. 4.

In cases of P-RWVG, Fig. 8(a) displays the distributions of the area-averaged k for the six selected Reynolds numbers with winglet vortex generators, mounted on the absorber plate, whilst Fig. 8(b) displays those with winglet vortex generators, mounted on the opposite insulation plate. Both figures show that the higher Reynolds number, the greater the k at the same elevation on the z-axis. The distributions in Fig 8(b) obviously mirror those in Fig. 8(a) on a horizontal axis. This is because the winglet vortex generators were repositioned from the upper absorber plate to the lower opposite insulation plate. For the reason that the distributions of area-averaged k in Fig. 8(b) skewed to the upper side where the absorber plate was, the diffusion (due to fluctuation) should be strong on this side. This enhanced heat transfer capability in the region adjacent to the absorber plate. Hence, just a small temperature difference between the absorber plate and the airflow was needed for the fixed q'' of the absorber plate. And, according to Eq. (4) and Eq. (5), the Nusselt number will be higher if the temperature difference $\left(\overline{T}_{sur} - \overline{T}_{air}\right)$ is smaller, since q'', D and K were constants in this work. Conversely, the distributions of area-averaged k in Fig. 8(a), skewing to the lower side, caused lower Nusselt numbers in the cases that winglet vortex generators were mounted on the opposite insulation plate. This was why all $\%diff_{Nu}$ values were positive and increased alongside Reynolds number in the P-RWVG case.

The distributions of area-averaged k for the RWVG case are displayed in Fig. 9(a) and Fig. 9(b). They were quite similar to those of P-RWVG, except their magnitudes were greater and their skewness was more distorted. Consequently, the $\%diff_{Nu}$ values of RWVG were greater than those of P-RWVG at the same Reynolds number.

The distributions of area-averaged k for the cases of P-TWVG in Fig. 10(a) and Fig. 10(b) could be used to confirm that the magnitudes of the area-averaged k and the skewness of area-averaged k distributions played an important role in $\%diff_{Nu}$. Both figures display both smaller magnitudes of area-averaged k and less distorted skewness of the area-averaged k distributions, which corresponds to the smaller $\%diff_{Nu}$ values of P-TWVG (compared to those of P-RWVG and RWVG).

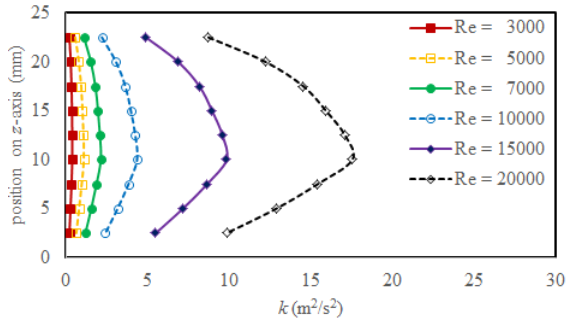

(a) Winglet vortex generator, installed on the absorber plate

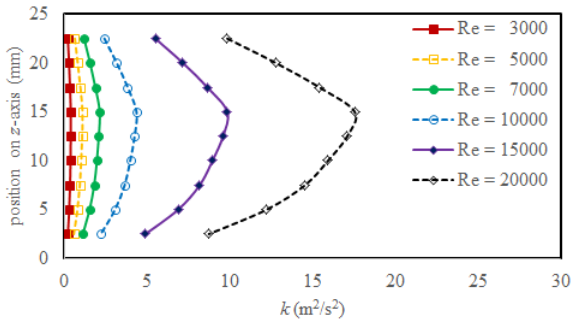

(b) Winglet vortex generator, installed on the opposite plate

Fig. 8 Distributions of area-averaged turbulent kinetic energy (k) against z-axis position in cases of P-RWVG.

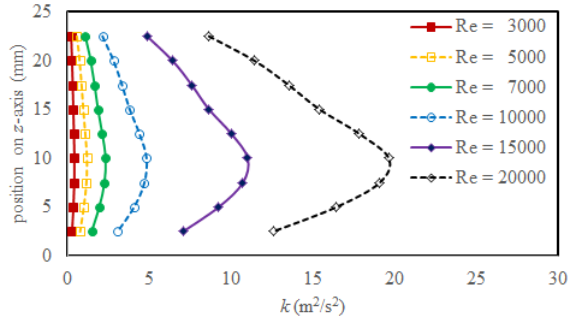

(a) Winglet vortex generator, installed on the absorber plate

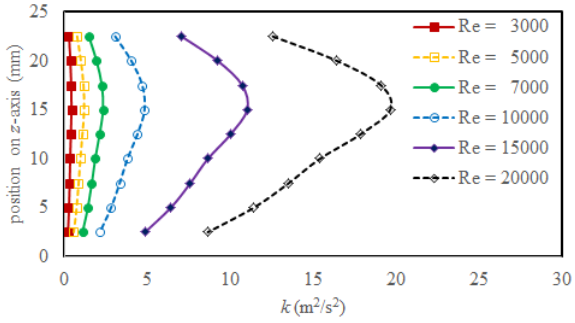

(b) Winglet vortex generator, installed on the opposite plate

Fig. 9 Distributions of area-averaged turbulent kinetic energy (k) against z-axis position in cases of RWVG.

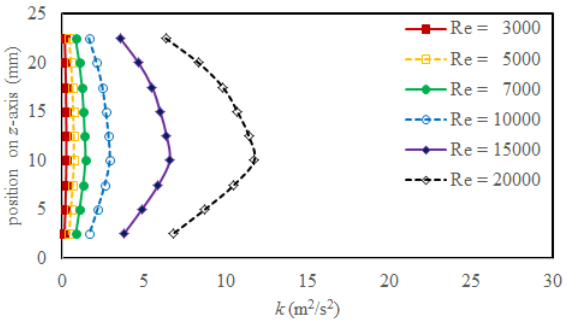

(a) Winglet vortex generator, installed on the absorber plate

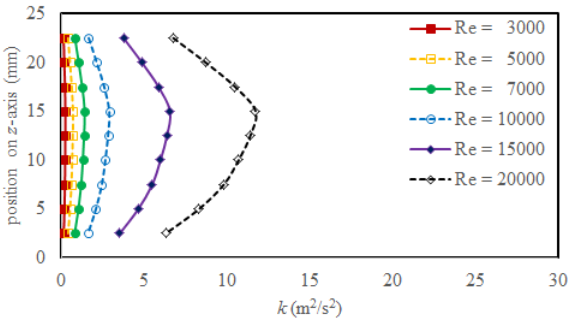

(b) Winglet vortex generator, installed on the opposite plate

Fig. 10 Distributions of area-averaged turbulent kinetic energy (k) against z-axis position in cases of P-TWVG.

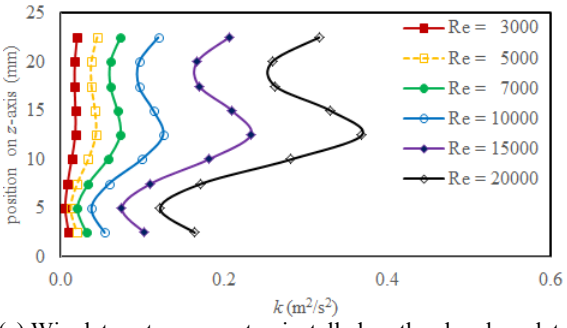

(a) Winglet vortex generator, installed on the absorber plate

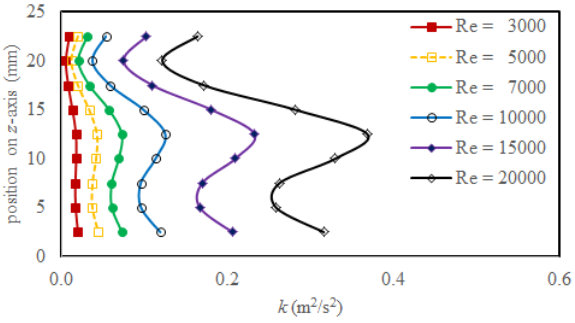

(b) Winglet vortex generator, installed on the opposite plate

Fig. 11 Distributions of area-averaged turbulent kinetic energy (k) against z-axis position in cases of TWVG.

The distributions of area-averaged k for TWVG were different to the previous three cases .However, the influence of area-averaged k could be minimal, as the magnitudes of the area-averaged k were very small in these cases. Heat transfer due to convection, thus, was the only factor, influencing $\%diff_{Nu}$.

5. CONCLUSION

The simulated results of the four winglet vortex generator shapes show that winglet vortex generator position in solar air heaters influence the capability of the heat transfer from the absorber plate to the air, flowing through the heat exchange duct .When winglet vortex generators were mounted on the opposite insulation plate, heat transfer between the absorber plate and airflows in the heat exchange duct was better with winglet vortex generators of P-RWVG, RWVG or P-TWVG design. However, the opposite result was obtained for TWVG as shown in Table 1.

Table 1 Values of $\%diff_{Nu}$ for the four different shapes of winglet vortex generator and the corresponding Reynolds numbers.

Re	$\%diff_{Nu}$			
	P-RWVG	RWVG	P-TWVG	TWVG
3000	33.3	45.1	6.8	6.2
5000	42.0	58.6	22.9	1.4
7000	49.3	70.1	25.6	-2.5
10000	50.3	76.7	30.6	-5.5
15000	48.5	75.2	29.5	-10.5
20000	47.3	75.9	28.9	-14.6

This could be explained by considering both the magnitudes of domain-averaged k and the skewness of area-averaged k distribution along the z-axis, i.e .heat transfer is better on the side to which the area-averaged k distribution skews. Results also show that the higher the domain-averaged k, the greater the $\%diff_{Nu}$ magnitude.

NOMENCLATURE

A_h	area of punched hole
A_w	area of winglet vortex generator
B_R	winglet blockage ratio
C_P	specific heat capacity of air
c	longer base of winglet vortex generator
c_s	shorter base of winglet vortex generator
D	hydraulic diameter
d	hole diameter
e	winglet vortex generator height
f	friction factor
H	duct height
h	heat transfer coefficient
K	thermal conductivity of air
k	turbulent kinetic energy
L	duct length
$\dot{m}$	rate of mass airflow
Nu	Nusselt number
P-RWVG	perforated rectangular winglet vortex generator
P-TWVG	perforated trapezoidal winglet vortex generator
P_l	length of longitudinal pitch
P_R	longitudinal pitch length ratio

P_t	length of transverse pitch
Pr	Prandtl number
q''	heat flux
Re	Reynolds number
RWVG	rectangular winglet vortex generator
SAH	solar air heater
TWVG	trapezoidal winglet vortex generator
u	velocity
W	duct width

Greek Symbols

$\%diff$	percentage of difference
ΔP	pressure drop
μ	dynamic viscosity of air
ρ	density of air

Subscripts

absorber	absorber plate
air	air
e	exit/efflux
f	friction factor
i	inlet/influx
Nu	Nusselt number
oposite	opposite insulation plate
sur	surface of absorber plate

REFERENCES

Abdullah, A.S., Amro, M.I., Younes, M.M., Omara, Z.M., Kabeel, A.E., Essa, F.A., 2020, "Experimental Investigation of Single Pass Solar Air Heater with Reflectors and Turbulators," *Alexandria Engineering Journal*, **59**, 579–587.
http://dx.doi.org/10.1016/j.aej.2020.02.004

Afshari, F., Sozen, A., Khanlari, A., Dogus, A., Tuncer, Sirin,C., 2020, "Effect of Turbulator Modifications on the Thermal Performance of Cost-Effective Alternative Solar Air Heater," *Renewable Energy*, **158**, 297–310.
http://dx.doi.org/10.1016/j.renene.2020.05.148

Agrawal, Y., Bhagoria, J., 2021, "Experimental Investigation for Pitch and Angle of Arc Effect of Discrete Artificial Roughness on Nusselt Number and Fluid Flow Characteristics of a Solar Air Heater," *Materials Today: Proceedings*, **46**, 5506–5511.
http://dx.doi.org/10.1016/j.matpr.2020.09.249

Aharwal, K.R., Gandhi, B.K., Saini, J.S., 2008, "Experimental Investigation on Heat-Transfer Enhancement Due to a Gap in an Inclined Continuous Rib Arrangement in a Rectangular Duct of Solar Air Heater," *Renewable Energy*, **33**, 585–596.
http://dx.doi.org/10.1016/j.renene.2007.03.023

Alam, T., Saini, R.P., Saini, J.S., 2014, "Effect of Circularity of Perforation Holes in V-Shaped Blockages on Heat Transfer and Friction Characteristics of Rectangular Solar Air Heater Duct," *Energy Conversion and Management*, **86**, 952–963.
http://dx.doi.org/10.1016/j.enconman.2014.06.050

Antony, A.L., Shetty, S.P., Madhwesh, N., Yagnesh Sharma, N., Vasudeva Karanth, K., 2020, "Influence of Stepped Cylindrical Turbulence Generators on the Thermal Enhancement Factor of a Flat Plate Solar Air Heater," *Solar Energy*, **198**, 295–310.
http://dx.doi.org/10.1016/j.solener.2020.01.065

Bansal, G., Kishore, C., Dogra, V., Bansal, A., Keshari, R., 2020, "Impact of Relative Roughness Height on the Materialistic Thermohydraulic Performance of the Multiple V-Ribbed Solar Air Heater," *Materials Today: Proceedings*, **26**, 1845–1849.
http://dx.doi.org/10.1016/j.matpr.2020.02.405

Barik, A.K., Mohanty, A., Senapati, J.R., Awad, M.M., 2021, "Constructal Design of Different Ribs for Thermo-Fluid Performance Enhancement of a Solar Air Heater (SAH)," *International Journal of Thermal Sciences*, **160**, 106655.
http://dx.doi.org/10.1016/j.ijthermalsci.2020.106655

Boulemtafes-Boukadoum, A., Absi, R., Abbassi, I.E., Darcherif, M., Benzaoui, A., 2019, "Numerical Investigation of Absorber's Roughness Effect on Heat Transfer in Upward Solar Air Heaters," *Energy Procedia*, **157**, 1089-1100.
http://dx.doi.org/10.1016/j.egypro.2018.11.276

Dezan, D.J., Rocha, A.D., Ferreira, W.G., 2020, "Parametric Sensitivity Analysis and Optimisation of a Solar Air Heater with Multiple Rows of Longitudinal Vortex Generators," *Applied Energy*, **263**, 114556.
http://dx.doi.org/10.1016/j.apenergy.2020.114556

Dezan, D.J., Rocha, A.D., Salviano, L.O., Ferreira, W.G., 2020, "Thermo-Hydraulic Optimization of a Solar Air Heater Duct with Non-Periodic Rows of Rectangular Winglet Pairs," *Solar Energy*, **207**, 1172–1190.
http://dx.doi.org/10.1016/j.solener.2020.06.112

Ebrahim Momin, A.-M., Saini, J.S., Solanki, S.C., 2002, "Heat Transfer and Friction in Solar Air Heater Duct with V-Shaped Rib Roughness on Absorber Plate," *International Journal of Heat and Mass Transfer*, **45**, 3383–3396.
http://dx.doi.org/10.1016/S0017-9310(02)00046-7

Eiamsa-ard, S., Promvonge, P., 2008, "Numerical Study on Heat Transfer of Turbulent Channel Flow over Periodic Grooves," *International Communications in Heat and Mass Transfer*, **35**, 844-852.
http://dx.doi.org/10.1016/j.icheatmasstransfer.2008.03.008

Ghritlahre, H.K., Chandrakar, P., Ahmad, A., 2020, "Application of ANN Model to Predict the Performance of Solar Air Heater Using Relevant Input Parameters," *Sustainable Energy Technologies and Assessments*, **40**, 100764.
http://dx.doi.org/10.1016/j.seta.2020.100764

Ghritlahre, H.K., Sahua, P.K., Chand, S., 2020, "Thermal Performance and Heat Transfer Analysis of Arc Shaped Roughened Solar Air Heater – An Experimental Study," *Solar Energy*, **199**, 173–182.
http://dx.doi.org/10.1016/j.solener.2020.01.068

Gopi, R., Ponnusamy, P., Fantin Arokiaraj, A., Raji, A., 2021, "Performance Comparison of Flat Plate Collectors in Solar Air Heater by Theoretical and Computational Method," *Materials Today: Proceedings*, **39**, 823–826.
http://dx.doi.org/10.1016/j.matpr.2020.09.809

Hassan, H., Yousef, M.S., Abo-Elfadl, S., 2021, "Energy, Exergy, Economic and Environmental Assessment of Double Pass V-Corrugated-Perforated Finned Solar Air Heater at Different Air Mass Ratios," *Sustainable Energy Technologies and Assessments*, **43**, 100936.
http://dx.doi.org/10.1016/j.seta.2020.100936

Hosseini, S.S., Ramiar, A., Ranjbar, A.A., 2019, "The Effect of Fins Shadow on Natural Convection Solar Air Heater," *International Journal of Thermal Sciences*, **142**, 280–294.
http://dx.doi.org/10.1016/j.ijthermalsci.2019.04.015

Komolafe, C.A., Oluwaleye, I.O., Awogbemi, O., Osueke, C.O., 2019, "Experimental Investigation and Thermal Analysis of Solar Air Heater Having Rectangular Rib Roughness on the Absorber Plate," *Case Studies in Thermal Engineering*, **14**, 100442.
http://dx.doi.org/10.1016/j.csite.2019.100442

Global Digital Central
ISSN: 2151-8629

Korpale, V.S., Deshmukh, S.P., Mathpati, C.S., Dalvi, V.H., 2020, "Numerical Simulations and Optimization of Solar Air Heaters," *Applied Thermal Engineering*, **180**, 115744.
http://dx.doi.org/10.1016/j.applthermaleng.2020.115744

Kumar, A., Layek, A., 2019a, "Energetic and Exergetic Performance Evaluation of Solar Air Heater with Twisted Rib Roughness on Absorber Plate," *Journal of Cleaner Production*, **232**, 617–628.
http://dx.doi.org/10.1016/j.jclepro.2019.05.363

Kumar, A., Layek, A., 2019b, "Nusselt Number and Fluid Flow Analysis of Solar Air Heater Having Transverse Circular Rib Roughness on Absorber Plate Using LCT and Computational Technique," *Thermal Science and Engineering Progress*, **14**, 100398.
http://dx.doi.org/10.1016/j.tsep.2019.100398

Kumar, A., Layek, A., 2020a, "Nusselt Number and Friction Characteristics of a Solar Air Heater That Has a Winglet Type Vortex Generator in the Absorber Surface," *Experimental Thermal and Fluid Science*, **119**, 110204.
http://dx.doi.org/10.1016/j.expthermflusci.2020.110204

Kumar, A., Layek, A., 2020b, "Nusselt Number and Friction Factor Correlation of Solar Air Heater Having Winglet Type Vortex Generator over Absorber Plate," *Solar Energy*, **205**, 334–348.
http://dx.doi.org/10.1016/j.solener.2020.05.047

Kumar, R., Goel, V., Singh, P., Saxena, A., Kashyap, A.S., Rai, A., 2019, "Performance Evaluation and Optimization of Solar Assisted Air Heater with Discrete Multiple Arc Shaped Ribs," *Journal of Energy Storage*, **26**, 100978.
http://dx.doi.org/10.1016/j.est.2019.100978

Liu, J., Xie, G., Simon, T.W., 2015, "Turbulent Flow and Heat Transfer Enhancement in Rectangular Channels with Novel Cylindrical Grooves," *International Journal of Heat and Mass Transfer*, **81**, 563–577.
http://dx.doi.org/10.1016/j.ijheatmasstransfer.2014.10.021

Luan, N.T., Phu, N.M., 2020, "Thermohydraulic Correlations and Exergy Analysis of a Solar Air Heater Duct with Inclined Baffles," *Case Studies in Thermal Engineering*, **21**, 100672.
http://dx.doi.org/10.1016/j.csite.2020.100672

Madhwesh, N., Vasudeva Karanth, K., Yagnesh, N., Sharma, 2019, "An Innovative Surface Morphology for a Solar Air Heater to Augment its Performance," *Procedia Manufacturing*, **35**, 1087-1095.
http://dx.doi.org/10.1016/j.promfg.2019.06.061

Mahanand, Y., Senapati, J.R., 2020, "Thermal Enhancement Study of a Transverse Inverted-T Shaped Ribbed Solar Air Heater," *International Communications in Heat and Mass Transfer*, **119**, 104922.
http://dx.doi.org/10.1016/j.icheatmasstransfer.2020.104922

Murali, G., Sai Nandan, B., Sampath Kumar Reddy, N., Teja, D., Kalyan Kumar, N., 2020, "Experimental Study on Double Pass Solar Air Heater with Fins at Lower and Upper Channel," *Materials Today: Proceedings*, **21**, 578–583.
http://dx.doi.org/10.1016/j.jksues.2012.05.004

Pandey, N.K., Bajpai, V.K., Varun, 2016, "Experimental Investigation of Heat Transfer Augmentation Using Multiple Arcs with Gap on Absorber Plate of Solar Air Heater," *Solar Energy*, **134**, 314–326.
http://dx.doi.org/10.1016/j.solener.2016.05.007

Patel, Y.M., Jain, S.V., Lakhera, V.J., 2020, "Thermo-Hydraulic Performance Analysis of a Solar Air Heater Roughened with Reverse NACA Profile Ribs," *Applied Thermal Engineering*, **170**, 114940.
http://dx.doi.org/10.1016/j.applthermaleng.2020.114940

Promvonge, P., Thianpong, C., 2008, "Thermal Performance Assessment of Turbulent Channel Flows over Different Shaped Ribs," *International Communications in Heat and Mass Transfer*, **35**, 1327–1334.
http://dx.doi.org/10.1016/j.icheatmasstransfer.2008.07.016

Saravanakumar, P.T., Somasundaram, D., Matheswaran, M.M., 2020, "Exergetic Investigation and Optimization of Arc Shaped Rib Roughened Solar Air Heater Integrated with Fins and Baffles," *Applied Thermal Engineering*, **175**, 115316.
http://dx.doi.org/10.1016/j.applthermaleng.2020.115316

Singh, A.P., Varun, Siddhartha, 2014, "Heat Transfer and Friction Factor Correlations for Multiple Arc Shape Roughness Elements on the Absorber Plate Used in Solar Air Heaters," *Experimental Thermal and Fluid Science*, **54**, 117–126.
http://dx.doi.org/10.1016/j.expthermflusci.2014.02.004

Singh, S., Negi, B.S., 2020, "Numerical Thermal Performance Investigation of Phase Change Material Integrated Wavy Finned Single Pass Solar Air Heater," *Journal of Energy Storage*, **32**, 102002.
http://dx.doi.org/10.1016/j.est.2020.102002

Skullong, S., Thianpong, C., Promvonge, P., 2015, "Effects of Rib Size and Arrangement on Forced Convective Heat Transfer in A Solar Air Heater Channel," *Heat Mass Transfer*, **51**, 1475–1485.
http://dx.doi.org/10.1007/s00231-015-1515-5

Skullong, S., Promthaisong, P., Promvonge, P., Thianpong, C., Pimsarn, M., 2018, "Thermal Performance in Solar Air Heater with Perforated-Winglet-Type Vortex Generator," *Solar Energy*, **170**, 1101–1117.
http://dx.doi.org/10.1016/j.solener.2018.05.093

Tamna, S., Skullong, S., Thianpong, C., Promvonge, P., 2014, "Heat transfer behaviors in a solar air heater channel with multiple V-baffle vortex generators," *Solar Energy*, **110**, 720–735.
http://dx.doi.org/10.1016/j.solener.2014.10.020

Tanda, G., 2004, "Heat Transfer in Rectangular Channels with Transverse and V-Shaped Broken Ribs," *International Journal of Heat and Mass Transfer*, **47**, 229–243.
http://dx.doi.org/10.1016/S0017-9310(03)00414-9

Thianpong, C., Chompookham, T., Skullong, S., Promvonge, P., 2009, "Thermal Characterization of Turbulent Flow in a Channel with Isosceles Triangular Ribs," *International Communications in Heat and Mass Transfer*, **36**, 712–717.
http://dx.doi.org/10.1016/j.icheatmasstransfer.2009.03.027

Wang, D., Liu, J., Liu, Y., Wang, Y., Li, B., Liu, J., 2020, "Evaluation of the Performance of an Improved Solar Air Heater with "S" Shaped Ribs with Gap," *Solar Energy*, **195**, 89–101.
http://dx.doi.org/10.1016/j.solener.2019.11.034

Xiao, H., Dong, Z., Liu, Z., Liu, W., 2020, "Heat Transfer Performance and Flow Characteristics of Solar Air Heaters with Inclined Trapezoidal Vortex Generators," *Applied Thermal Engineering*, **179**, 115484.
http://dx.doi.org/10.1016/j.applthermaleng.2020.115484